ORIGINAL ARTICLE

Journal of Neurochemistry · JNC · The Official Journal of the International Society for Neurochemistry · WILEY

Expression of glucose transporter-2 in murine retina: Evidence for glucose transport from horizontal cells to photoreceptor synapses

Ming Yang[1,2,3] | Yiyi Chen[4] | Stavros Vagionitis[5] | Elöd Körtvely[6] |
Marius Ueffing[4] | Oliver Schmachtenberg[7] | Zhulin Hu[1,2] | Kangwei Jiao[1,2] |
François Paquet-Durand[4]

[1]Affiliated Hospital of Yunnan University & 2nd People's Hospital of Yunnan Province, Kunming, China

[2]Yunnan Eye Institute & Key Laboratory of Yunnan Province, Kunming, China

[3]1st Affiliated Hospital of Kunming Medical University, Kunming, China

[4]Institute for Ophthalmic Research, Eberhard-Karls-Universität, Tübingen, Germany

[5]Institute of Neuronal Cell Biology, Technical University of Munich, Munich, Germany

[6]Roche Pharma Research and Early Development, Immunology, Infectious Diseases and Ophthalmology (I2O), Discovery and Translational Area, Roche Innovation Center Basel, F. Hoffmann-La Roche Ltd, Basel, Switzerland

[7]CINV, Instituto de Biología, Facultad de Ciencias, Universidad de Valparaíso, Valparaíso, Chile

Correspondence
Kangwei Jiao, Affiliated Hospital of Yunnan University & 2nd People's Hospital of Yunnan Province, 650500 Kunming, China.
François Paquet-Durand, Institute for Ophthalmic Research, Eberhard-Karls-Universität 72076 Tübingen, Germany.
Email: francois.paquet-durand@klinikum.uni-tuebingen.de; kangwei.jiao@ynu.edu.cn

Abstract

The retina has the highest relative energy consumption of any tissue, depending on a steady supply of glucose from the bloodstream. Glucose uptake is mediated by specific transporters whose regulation and expression are critical for the pathogenesis of many diseases, including diabetes and diabetic retinopathy. Here, we used immunofluorescence to show that glucose transporter-2 (GLUT2) is expressed in horizontal cells of the mouse neuroretina in proximity to inner retinal capillaries. To study the function of GLUT2 in the murine retina, we used organotypic retinal explants, cultivated under entirely controlled, serum-free conditions and exposed them to streptozotocin, a cytotoxic drug transported exclusively by GLUT2. Contrary to our expectations, streptozotocin did not measurably affect horizontal cell viability, while it ablated rod and cone photoreceptors in a concentration-dependent manner. Staining for poly-ADP-ribose (PAR) indicated that the detrimental effect of streptozotocin on photoreceptors may be associated with DNA damage. The negative effect of streptozotocin on the viability of rod photoreceptors was counteracted by co-administration of either the inhibitor of connexin-formed hemi-channels meclofenamic acid or the

----

blocker of clathrin-mediated endocytosis dynasore. Remarkably, cone photoreceptors were not protected from streptozotocin-induced degeneration by neither of the two drugs. Overall, these data suggest the existence of a GLUT2-dependent glucose transport shuttle, from horizontal cells into photoreceptor synapses. Moreover, our study points at different glucose uptake mechanisms in rod and cone photoreceptors.

KEYWORDS
apoptosis, diabetes, diabetic retinopathy, energy metabolism, horizontal cells

1 | INTRODUCTION

The energy metabolism of neural tissues depends to a large extent on the adequate supply and uptake of glucose. This is particularly true for the retina, which has the highest relative energy consumption of any mammalian tissue (Lund-Andersen, 1979; Trick & Berkowitz, 2005). The uptake of glucose requires the expression of specific transporters, collectively referred to as glucose transporters (GLUTs). To date, research on GLUTs in the retina has focused on GLUT1, which is strongly expressed in barrier tissues, including in the retinal pigment epithelium (RPE) (Mantych et al., 1993). GLUT2 has been far less studied, although it has been suggested to play a role in the regulation of retinal blood glucose levels (Watanabe et al., 1999).

GLUT2 is a low affinity (K_m ~17 mM), high capacity transporter (Thorens, 2015), expressed at high levels in pancreatic beta-cells, in the basolateral membranes of intestinal and kidney epithelial cells, and in hepatocytes (Bell et al., 1990). Studies on GLUT2-deficient mice have indicated that GLUT2 may be required for the function of glucose sensors present in the central nervous system (Thorens, 2015). Therefore, studies of the expression of GLUT2 in neuronal tissues may lead to a better understanding of how exactly glucose operates as a metabolic regulatory signal (Koepsell, 2020). This could be especially relevant for retinal metabolism and the pathogenesis of neuroretinal diseases. For instance diabetic retinopathy (DR), a common complication of diabetes, is associated with a variety of pathophysiological events such as microaneurysms, neovascularization and photoreceptor degeneration, which eventually lead to irreversible blindness (Cai & Boulton, 2002).

The retina harbours two types of photoreceptors: Rods, which are responsible for vision at night, and cones, which mediate colour vision under daylight conditions (Power et al., 2020). In most mammals, including humans and mice, around 96% of photoreceptors are rods, with the remainder being cones (Peichl, 2005). Intriguingly, an early symptom of neuroretinal degeneration in DR patients appears to be cone degeneration and accordingly, the macula, *that is* the central area of the human retina that has the highest density of cones, is often strongly affected in DR. The opposite case for retinal diseases may be retinitis pigmentosa (RP), a rare, hereditary disease, which usually starts in the retinal periphery. In RP, the rod photoreceptors are afflicted by a genetic defect that causes their degeneration. This primary loss of rods entails a secondary degeneration of—genetically intact and fully functional—cones, eventually leading to complete blindness. It has been hypothesized that the loss of rods causes alterations in the uptake of glucose in cones, which could thus explain the progression of secondary cone photoreceptor loss in RP (Ait-Ali et al., 2015; Kanow et al., 2017).

One of the most studied animal models for RP is the *rd1* mouse (Keeler, 1924), characterized by a mutation in the *Pde6b* gene (Bowes et al., 1990). This leads to a rapid loss of rod photoreceptors within the first three post-natal weeks, followed by a secondary loss of cones and blindness by post-natal day 30.

Here, we show that in the mouse retina GLUT2 was strongly expressed in horizontal cells (HCs), located adjacent to inner retinal blood vessels running through the outer plexiform layer. There were no obvious expression differences for GLUT2 between healthy, wild-type (WT) and *rd1* mutant animals, indicating that GLUT2 was not expressed in photoreceptors. To test for the retinal function of GLUT2, we exposed organotypic retinal explant cultures to streptozotocin, a cytotoxic drug that is transported exclusively by GLUT2 (Szkudelski, 2001). Remarkably, STZ treatment resulted in degeneration of rods and cones, while leaving HCs essentially unaffected. The STZ-induced rod degeneration was prevented by co-treatment with meclofenamic acid, a blocker of connexin-formed gap junctions/hemi-channels, or the inhibitor of clathrin-mediated endocytosis dynasore. However, these treatments could not avert the deleterious effects of STZ on cone photoreceptors. Taken together, our data are consistent with a transport pathway that allows for the shuttling of glucose from HCs to photoreceptors.

2 | MATERIALS AND METHODS

2.1 | Animals

C3H HeA *Pde6b^rd1/rd1* (*rd1*) and congenic C3H HeA *Pde6b^+/+* wild-type (WT) mice were used, two mouse lines that were originally created in the lab of Somes Sanyal at the University of Rotterdam (Sanyal & Bal, 1973). All efforts were made to minimize the number of animals used and their suffering, notably through the use of in vitro experimentation (see below) and the use of both retinae from the same animal. Animals were housed in the specified pathogen-free (SPF) facility of the Tübingen Institute for Ophthalmic Research, under standard white cyclic lighting in type-2 long cages with a maximum of five adults per cage. They had free access to food

and water and were used irrespective of sex. Protocols compliant with the German law on animal protection were reviewed and approved by the 'Einrichtung fur Tierschutz, Tierärztlichen Dienst und Labortierkunde' of the University of Tübingen (AK 02–19 M, notice acc. to §4 German law on animal protection from 26.11.2015) and were in compliance with the association for research in vision and ophthalmology (ARVO) statement for the use of animals in vision research. A total of 72 mice were used for this study (37 mice for immunofluorescence and 35 mice for explant cultures).

2.2 | Cell death detection (TUNEL assay)

Fixed slides were dried at 37°C for 30 min and washed in phosphate-buffered saline (PBS) solution at room temperature (RT, 21°C), for 15 min. Afterwards, the slides were placed in TRIS buffer with proteinase K at 37°C for 5 min to inactivate nucleases. The slides were then washed with TRIS buffer (10 mM TRIS-HCL, pH 7.4), three times for 5 min each. Subsequently, the slides were placed in ethanol-acetic acid mixture (70:30) at −20°C for 5 min followed by three washes in TRIS buffer and incubation in blocking solution (10% normal goat serum, 1% bovine serum albumin, 1% fish gelatin in 0.1% PBS-Triton X100) for 1 h at RT (21°C). Lastly, the slides were placed in the terminal dUTP-nick-end labelling (TUNEL) solution (labelling with either fluorescein or tetra-methyl-rhodamine; Roche Diagnostics GmbH) in 37°C for 1 h and covered in Vectashield with DAPI (Vector) thereafter.

2.3 | Immunofluorescence and immunohistochemistry

Fixed slides were dried at 37°C for 30 min and rehydrated for 10 min in PBS at RT (21°C). For immunofluorescent labelling, the slides were incubated with blocking solution (10% normal goat serum, 1% bovine serum albumin in 0.3% PBS-Triton X 100) for 1 h at RT (21°C). The primary antibodies were diluted (see Table 1) in blocking solution and incubated at 4°C overnight. The slides were then washed

with PBS, three times for 10 min each. Subsequently, the secondary antibody, diluted in PBS (see Table 1), was applied to all slides and incubated for 1 h at RT (21°C). Lastly, the slides were washed with PBS and covered in Vectashield with DAPI (Vector).

For whole-mount staining, after removing the cornea, lens and sclera, four to five radial incisions were made in the retina. Retinae were fixed with 4% paraformaldehyde (PFA) for 15 min at RT (21°C) and washed three times with PBS. Retinae were then incubated in blocking solution (10% normal goat serum, 1% bovine serum albumin in 0.3% PBS-Triton X 100) for 1 h at RT (21°C). This was followed by incubation with primary antibodies for 4 days, washing in PBS for 1 h, and incubation with secondary antibody for 24 h. Finally, the retinae were washed in PBS overnight before being coverslipped with mounting media (Vectashield) and sealed with nail polish.

For poly-ADP-ribose (PAR) immunohistochemical staining, the fixed slides were placed in quenching solution (9% of 30% H_2O_2, 36% methanol, 55% of 0.3% PBS-Triton X100) for 20 min at RT (21°C) to reduce endogenous peroxidase activity and prevent false-positive results. Subsequently, the slides were washed with PBS, three times for 5 min each. Afterwards, the slides were incubated in blocking solution (10% normal goat serum in 0.3% PBS-Triton X100) at RT (21°C) for 30 min, then the PAR antibody (1:100 in blocking solution) was incubated overnight at 4°C. After washing in PBS, the biotinylated secondary antibody from the ABC peroxidase kit (Vector) was diluted in blocking solution and added onto the slides and incubated at RT (21°C) for 1 h. After washing with PBS, the ABC staining solution from the ABC peroxidase kit was applied and incubated for 1 h. After washing again with PBS, the slides were placed in DAB solution from ABC peroxidase kit at RT (21°C) for 2 min and 30 s followed by immediate PBS washing. The slides were then mounted with Aquatex (Sigma; 1.08562).

2.4 | Antibody validation by immunoprecipitation and mass spectrometry (IP-MS)

Retinae from five animals were homogenized in 500 μl lysis buffer (150 mM NaCl, 50 mM Tris-HCl pH 7.4, 0.5% NP-40 in the presence

TABLE 1 Primary and secondary antibodies used in the study, providers and dilutions

Antibody, species	RRID, Provider, cat. no.	1st antibody dilution	2nd antibody dilution
Rabbit polyclonal anti-GLUT2	AB_880234, Abcam, cat. no. 54460	1:200	1:350
Mouse monoclonal anti-calbindin D-28K (clone CB300)	Swant, cat. no. CB300	1:500	1:350
Mouse monoclonal anti-von Willebrand Factor (vWF; clone F8/86)	AB_2216702, Dako, cat. no. M0616	1:50	1:500
Mouse monoclonal anti-PAR (clone 10H)	AB_2272987, Enzo, cat. no. ALX-804-220	1:100	1:150
Rabbit anti-cone arrestin	AB_1163387, Sigma, cat. no. AB15282	1:500	1:350

of complete protease inhibitor cocktail, Roche Diagnostics). Fifty microlitres (500 µg) lysate was incubated with 5 µl GLUT2 antibody (Abcam ab54460) in 500 µl PBS on a rotator for 30 min at RT (21°C). Normal non-immune serum was used as negative control. Next, 25 µl Protein G magnetic beads (Pierce) were added and the incubation was continued for 15 min at RT (21°C). The beads were collected using a magnet (DynaMag™-2, Thermo Fisher) and intensively washed with PBS. Bound proteins were subjected to on-bead tryptic digestion followed by LC-MS/MS analysis performed on an UltiMate 3000 RSLCnano HPLC system (Dionex) coupled to an Orbitrap Fusion mass spectrometer (Thermo Fisher Scientific) by a nanospray ion source. All acquired spectra were processed and analysed using Mascot (Matrix Science, version 2.5.1; RRID:SCR_014322) and the human-specific Swiss-Prot database (rel. 2015/11/11). Mascot was searched with a fragment ion mass tolerance of 0.50 Da and a parent ion tolerance of 10.0 PPM. Carboxymethylation of cysteine was specified in Mascot as a fixed modification. Deamidation of asparagine and glutamine and oxidation of methionine were specified as variable modifications. Scaffold (v4.4.8, Proteome Software Inc.) was used to validate MS/MS-based peptide and protein identifications.

2.5 | Retinal explant cultures

The retinal explantation procedure and long-term cultivation in a defined medium, free of serum and antibiotics, is described in detail in (Belhadj et al., 2020). Briefly, retinal explantation was performed in the late morning, immediately after the decapitation of post-natal day (P) 5 WT animals. The heads were cleaned with 70% ethanol, the eyes were removed under aseptic conditions and placed into R16 basal medium (BM; Gibco, Paisley, UK; cat. no.: 047-90743A). Afterwards the eyes were washed for 5 min, followed by a 15 min incubation in 0.12% Proteinase K (Sigma-Aldrich Chemie GmbH, Taufkirchen, Germany; cat. no.: P6556) at 37°C to predigest the sclera and to allow for an easy separation of the retina together with its retinal pigment epithelium. Then, the eyes were placed for 5 min in BM with 10% foetal calf serum to deactivate Proteinase K. Under the microscope and sterile conditions, the anterior segment, lens and vitreous body were carefully removed from the eyeballs, the optic nerve was cut, and the retinae were removed from the sclera. Four incisions were made into the retina to give a flat, clover leaf-like structure that was transferred to a culturing membrane (sterile 24 mm insert with 0.4 µm polycarbonate membrane, Corning-Costar; cat. no.: 3412), with the ganglion cell layer facing up. Subsequently, culturing membranes were placed in six-well culture plates (BD Biosciences) and incubated in 1.3 ml of R16 complete medium (CM) with supplements (Caffe et al., 2001), at 37°C in a humidified incubator with 5% CO_2. The CM was changed every 2 days (Figure 1).

To functionally confirm the expression of GLUT2 in the retina, the retinal explant cultures were treated with streptozotocin (STZ), an alkylating antineoplastic agent selectively transported by GLUT2. WT mouse retinal explants were prepared at P5, explants derived from left and right eyes of a given animal were separated into two

groups and numbered consecutively. Starting with the 'Left' group, 16 to 30 retinal explants (from 8–15 animals) were randomly assigned to one of the four or six treatment groups by rolling a die. Each of the eyes on the die corresponded to one of the treatment groups. The 'Right' retinae were then similarly assigned by rolling a die, however, assignment was always such that the two retinae from one animal were always allocated to different groups. Retinae were exposed to different concentrations of STZ (1.5, 8 and 15 mM) from P7 to 11. STZ (Sigma; S0130) solution was always freshly prepared by first dissolving 40 mg STZ in 1 ml of CM. This 150 mM STZ stock solution was further diluted in CM at a ratio of 1:10 for 15 mM STZ, 1:18.75 for 8 mM STZ and 1:100 for 1.5 mM STZ. At P7 and P9 freshly prepared STZ was added to the R16 medium, the culturing period ended at P11 with fixation of the retina in 4% PFA, cryoprotection in graded sucrose solutions (10, 20, 30%), and subsequent cryosectioning (12 µm) in a Leica Biosystems CM cryostat. Meclofenamic acid sodium salt (100 µM; Sigma; M4531) and dynasore hydrate (50 µM; Sigma; D7693) were added together with STZ.

To simulate type-1 (T1DM) or type-2 diabetes mellitus (T2DM) conditions, 34 mM glucose without insulin (T1DM) or 20 mM 2-deoxy-glucose (T2DM) was added to the R16 medium. Retinal explants were subjected to T1DM conditions for four days, from P7 to P11, while to simulate T2DM the 2-deoxy-glucose treatment was applied for 24 h from P10 to P11. No blinding of treatment groups was performed.

2.6 | Microscopy, cell counting and statistical analysis

Fluorescence microscopy was performed with a Z1 Apotome microscope equipped with a Zeiss Axiocam digital camera (Zeiss, Oberkochen, Germany; RRID:SCR_013672). Images were captured using Zen software (Zeiss; RRID: SCR_018163) and the Z-stack function (14-bit depth, 2752*2208 pixels, pixel size = 0.227 µm, 9 Z-planes at 1 µm steps) and were taken from central areas of the retina. The raw images were converted into maximum intensity projections using Zen software. Confocal imaging of whole-mount retina was performed on a Leica TCS SP8 microscope (Leica Microsystems IR GmbH, Germany). Raw images were processed in Fiji software (RRID:SCR_002285) by linear adjustment of brightness and contrast and saved as TIFF files. Confocal Z-stack images were converted into maximum intensity projections, the brightness and contrast were adjusted linearly, and images were saved as TIFF files.

Photoreceptors stained by the TUNEL assay were counted manually on three images per explant, the average cell number in a given ONL area was estimated based on DAPI staining and used to calculate the percentage of TUNEL-positive cells. Fluorescence intensity data were obtained using the built-in image profile function in Zen Software (Zeiss). Adobe Photoshop CS6 (Adobe Systems Incorporated; RRID:SCR_014199) and Adobe Illustrator CC 2019 software (RRID:SCR_010279) were used for primary image processing. All data given represent the means and standard deviation from

FIGURE 1 Timeline, experimental groups and number of retinae per condition. Retinal cultures were started by explantation at post-natal day (P) 5, serum-free R16 medium was changed every 2 days, and the cultures were stopped by fixation at P11. *Note that retinae from individual animals were assigned to different experimental groups

	Control	[n = 4-8 retinae *; *cf*. Fig. 5]
	Control	[n = 5-8 retinae *; *cf*. Fig. 6]
	Control	[n = 3 retinae *; *cf*. Supp. Fig. 2]
	STZ 1.5mM/8mM/15mM	[n = 4 retinae per group *; *cf*. Fig 5]
	STZ 15mM	[n = 6 retinae per group *; *cf*. Fig 6]
No treatment (adaptation to culture)	MFA/STZ+MFA/DYN/STZ+DYN	[n = 5 retinae per group *; *cf*. Fig 6]
	High glucose, no insulin	[n = 3 retinae per group *; *cf*. Supp. Fig 2]
No treatment	2-deoxyglucose	[n = 3 retinae per group *; *cf*. Supp. Fig 2]

P5 — Retinal explantation
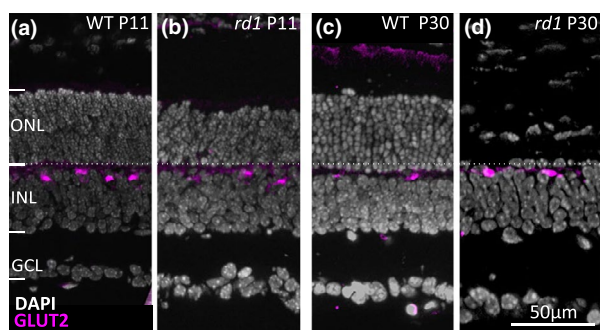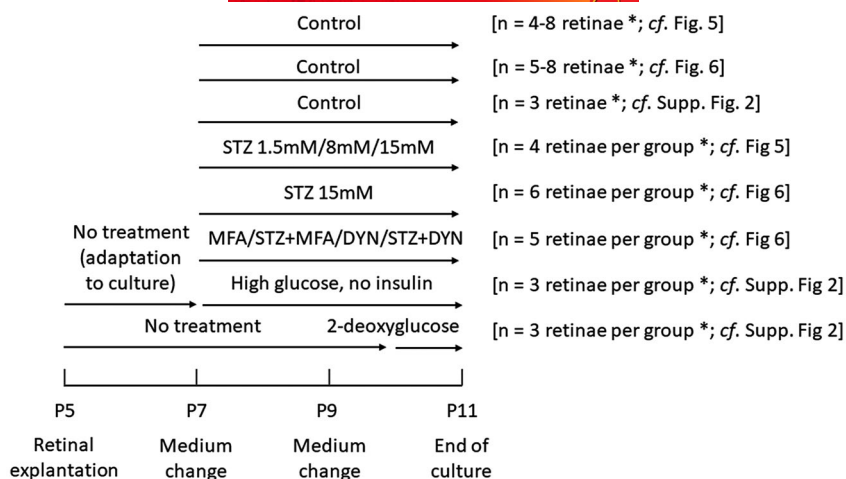P7 — Medium change
P9 — Medium change
P11 — End of culture

FIGURE 2 GLUT2 is expressed in wild-type and *rd1* mutant outer retina. Immunostaining for GLUT2 (magenta) was performed in wild-type (WT) and degenerating *rd1* retina, at post-natal (P) day 11 and 30. DAPI (grey) was used as a nuclear counterstain. (a, b) At P11, in both WT and *rd1*, a strong GLUT2 labelling was seen at the outer border of the inner nuclear layer (INL, dotted line), and at the level of the outer plexiform layer (OPL). (c, d) At P30, the WT presented the normal morphology of the outer nuclear layer (ONL) and INL, while almost all photoreceptors had been lost in the *rd1* retina. Nonetheless, the GLUT2 labelling in the OPL was present in both genotypes. GCL, ganglion cell layer. Images are representative for labelling performed on retinae from at least four different animals per genotype and time-point

at least four different animals. The study was not pre-registered. The study is exploratory. Group sizes were defined based on prior experience (Vighi et al., 2018), no sample calculation was performed. Only samples without contamination were included in the study. No animals were excluded during experiments. The replicate number n refers to individual animals or independent retinal explant culture preparations. Statistical comparisons between experimental groups were made using Student´s paired t-test (*cf*. Figure 4) or ANOVA and multiple comparisons correction (*cf*. Figures 5, 6) using Graph Pad Prism 9.1 for Windows (Graph Pad Software). Assessment of the normality (Shapiro–Wilk test) of the data and testing for outlier (Grubbs' test) was performed using Graph Pad Prism 9.1 (RRID: SCR_002798). Levels of significance were as follows: $*p < 0.05$; $**p < 0.01$; $***p < 0.001$. For full statistical reports on these analyses please see Tables S1–S3.

3 | RESULTS

3.1 | GLUT2 expression in the outer plexiform layer of the mouse retina

While a previous study reported the presence of GLUT2 in the apical ends of retinal Müller cells in rat (Watanabe et al., 1994), altogether very little is known about the expression of GLUT2 in the mammalian retina. To assess possible links between GLUT2 and retinal disease, we first conducted GLUT2 immunofluorescent labelling, in both WT mice and in the *rd1* photoreceptor degeneration mutant (Power et al., 2020). In both genotypes, at post-natal day (P) 11 and 30, we found prominent GLUT2 expression at the level of the outermost inner nuclear layer (INL), suggesting a possible expression in horizontal cell (HC) somata (Figure 2). Occasionally, a very faint GLUT2 staining was seen also in photoreceptor outer segments, however, given the strong density of lipid membranes in these structures, this labelling was likely unspecific. While the *rd1*-induced degeneration of photoreceptors progressed markedly from P11 to P30, resulting in a near-complete loss of the outer nuclear layer by P30, no specific differences in GLUT2 immunoreactivity between WT and *rd1* mice were observed at that age (Figure 2c, d). The latter result strongly suggested that GLUT2 expression was not linked to photoreceptors.

GLUT2 staining on retinae from 11- to 24-week-old animals further confirmed its expression on HCs for both WT and *rd1* genotypes (Figure S1). Moreover, we used an in vitro model for diabetic retinopathy (Valdes et al., 2016) to show that also in diabetic retina HCs express the GLUT2 transporter (Figure S2).

3.2 | GLUT2 antibody validation by immunoprecipitation and mass-spectrometry

The GLUT2 antibody used in our study (Abcam ab54460; RRID: AB_880234) had been validated in previous studies, including for western blot and immunofluorescence (Chen et al., 2018; Koukourakis et al., 2016). Nevertheless, we further tested for

specificity for GLUT2 using immunoprecipitation followed by subsequent identification of precipitated proteins with mass spectrometry (IP-MS). The IP-MS analysis demonstrated that the GLUT2 antibody was able to specifically precipitate its target protein. Also, GLUT2 was absent from the list of precipitated proteins in the negative control experiment using normal (non-immune) serum. The IP-MS results thus confirm that the protein detected in our immunofluorescence staining was indeed GLUT2.

3.3 | GLUT2 expression in horizontal cells (HCs)

With the specificity of the GLUT2 antibody established by IP-MS, we proceeded to test whether the GLUT2 staining observed in the outer plexiform layer (OPL) was associated with HCs. To this end, we performed a co-immunostaining for the Ca^{2+}-binding protein calbindin, a marker for HCs in the mouse retina (Haverkamp & Wassle, 2000). In the adult, P30 mouse retina, this staining revealed essentially a complete co-localization in the OPL, confirming that HCs were expressing GLUT2 (Figure 3a, b). Since, in the INL, calbindin is also expressed in certain amacrine cells (Kovács-Öller et al., 2019) the colocalization between GLUT2 and calbindin was not complete, with 68.2% (±19.8, n = 3) of calbindin-labelled cells also being positive for GLUT2. Within individual HCs, GLUT2 was predominantly localized in the cytoplasm, surrounding the nucleus, and in the dendritic processes along the OPL (Figure 3c, d). However, in the inner

retina, GLUT2 labelling did not co-localize with calbindin-stained amacrine cells and ganglion cell structures. For a 3D rendering of GLUT2 and calbindin labelling see Video S1.

3.4 | GLUT2-positive horizontal cells are close to inner retinal blood vessels

The localization of GLUT2 to HCs raised the question as to how glucose could reach HCs and whether the GLUT2-positive HCs were in physical contact with the inner retinal vasculature. While this had been suggested in earlier works (Mojumder, 2008; Usui et al., 2015), we wanted to address this question via immunostaining for the von Willebrand factor (vWF), a marker for blood vessels (Figure S3). In whole-mount retina vWF immunostaining provided for a strong labelling of blood vessels in the inner retina and revealed an average blood vessel diameter of 2.9 ± 0.88 μm (±SD; n = 26 blood vessels). Based on the somatic calbindin staining, the diameter of the HC soma was found to be 9.7 μm (±0.94, n = 27). For a 3D reconstruction of a representative GLUT2 and vWF labelling see Video S2.

To study the distribution and relative localization of HCs and blood vessels more closely, the distance from HC somata to blood vessels was measured in retinal whole-mount preparations as the space between the edge of a calbindin-positive cell and the nearest blood vessel. In the OPL, 27.8% (±12.3, n = 10 images obtained from 4 different whole-mount retinae) of all HC somata were directly
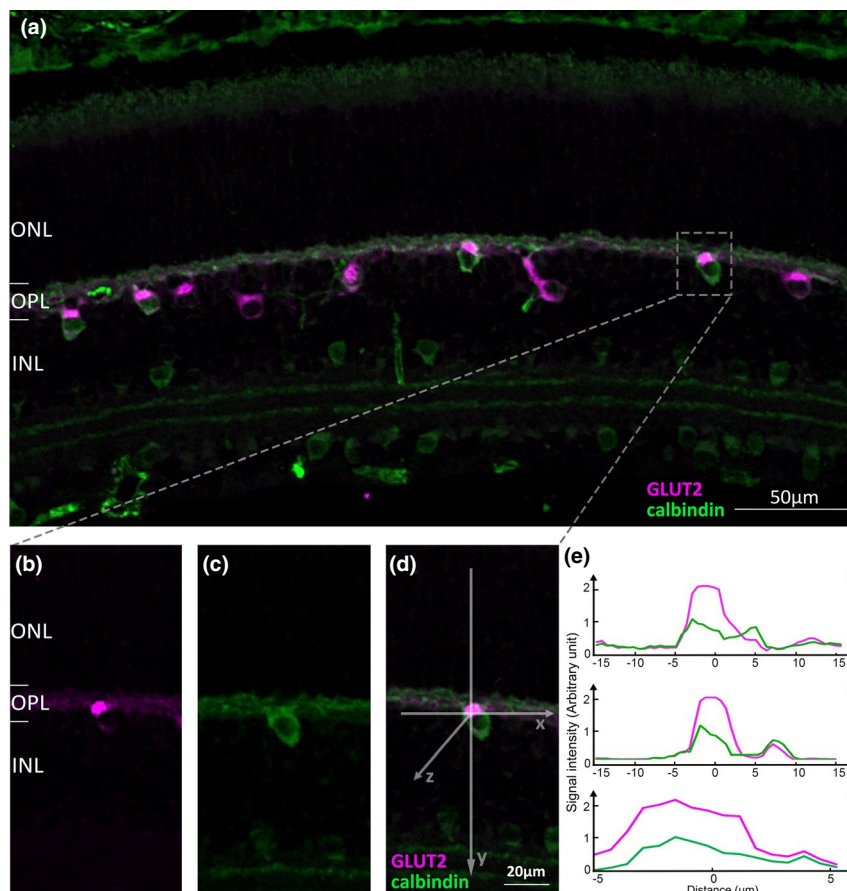

FIGURE 3 GLUT2 is expressed in retinal horizontal cells. (a) Co-immunostaining for GLUT2 (magenta) and the horizontal cell (HC) marker calbindin (green) showed GLUT2 expression mostly at the outer end of HCs, and in HC dendrites lining the outer plexiform layer (OPL). (b–d) Higher magnification of a single GLUT2-positive HC. (e) Co-localization of GLUT2 and calbindin was further illustrated by a signal intensity plot along the x-, y- and z-axis, showing a spatial overlap between magenta (GLUT2) and green (calbindin) curves. ONL, outer nuclear layer, INL, inner nuclear layer. Images are representative for labelling performed on retinae from four different WT animals

contacting vessels, while another 51.5% ($\pm$14.1, $n = 10$) of the HCs resided in close proximity to blood vessels, within one vessel diameter (Figure 4a). Additionally, we also measured the distances from the centre of a GLUT2-positive structure (i.e. inside a HC) to the nearest vWF-positive blood vessel (Figure 4b). In this comparison, 13.2% ($\pm$9.2, $n = 10$) of all GLUT2-positive structures were in direct contact with a vWF-positive blood vessel, whereas 35.9% ($\pm$10.1, $n = 10$) of GLUT2-labelling was localized within one vessel diameter. The average distance between a calbindin-positive HC soma and a blood vessel was 5.0 μm ($\pm$1.9, $n = 10$), the average GLUT2 to vWF distance was 8.0 μm ($\pm$2.5, $n = 10$).

To assess whether HCs were indeed contacting blood vessels, for each image captured, the colour channel displaying blood vessels (i.e. the green channel in Figure 4b, c) was rotated by 90 degrees and the HC/GLUT2 to blood vessel distance was measured again. When the 0° and 90° values were compared (Figure 4d) no statistically significant differences were found, neither for the calbindin-label-based assessment nor for the GLUT2/vWF-based evaluation. However, the number of HCs either in direct contact or in close vicinity to blood vessels was similar for both 0° (see above) and 90° (for calbindin label: 33.5% $\pm$9.4, $n = 10$; 55.8% $\pm$ 9.4, $n = 10$; for GLUT2/vWF label: 16.8% $\pm$ 8.3, $n = 10$; 33.8% $\pm$ 8.8, $n = 10$).

Taken together, the localization of HCs and inner retinal blood vessels suggested that the density of both capillary network in the OPL and the HC network was high enough so that HCs were always near a vessel. However, at this point, this analysis does not allow to conclusively assess whether HCs are in direct contact with capillaries.

3.5 | STZ induces cell death in the outer nuclear layer of the mouse retina

After establishing the close relationship between HCs and retinal blood vessels, we went on to confirm retinal GLUT2 expression physiologically. To this end, we used streptozotocin (STZ), a compound that is selectively transported and internalized into cells by GLUT2 (Szkudelski, 2001). STZ is a DNA alkylating agent and is used as an antibiotic and anti-neoplastic drug that is approved for the treatment of cancer of pancreatic islet cells (Halperin et al., 2015). STZ is highly toxic to cells expressing GLUT2 and is widely used in diabetes research to ablate GLUT2-expressing pancreatic islet cells, abolishing insulin production and rendering animals rapidly type-1 diabetic (Brosky & Logothetopoulos, 1969; Furman, 2015; Schnedl et al., 1994).

To test for the effects of STZ on the mouse retina, we used organotypic retinal explants cultured under defined, serum-free conditions (Belhadj et al., 2020; Vighi et al., 2018). Retinal culture started with explantation at P5, and the explants were exposed to STZ from P7 to 11 (*cf.* Figure 1). While retina cultured in vitro displays a somewhat higher level of cell death than the *in vivo* retina, untreated WT retinal explants remain stable over at least 2 weeks of culture (Belhadj et al., 2020; Calbiague et al., 2020).

Given the expression pattern of GLUT2, our expectation was that STZ would selectively ablate HCs. Surprisingly, when explanted

retina was treated with STZ, at concentrations typically used in diabetes research (i.e. 15 mM), the GLUT2-expressing HCs were not visibly affected (Figure 5a–d). A quantification of calbindin-positive cell bodies in the outer retina also revealed no effects of STZ on HC viability (Figure 5q). However, photoreceptors were ablated selectively and dose dependently as evidenced by the thickness of the ONL, which decreased sharply with rising STZ concentrations, while the inner retina appeared to be unaffected (Figure 4e–h, quantification in R). Similarly, the TUNEL assay showed a strong increase in cell death in the ONL with rising STZ concentration (Figure 5s). Remarkably, this effect on photoreceptor viability appeared to be even more marked in cones, which disappeared completely already at the intermediate 8 mM STZ level (Figure 5i–l, quantification in T). Furthermore, there was an increase in ONL cells positive for poly-ADP-ribosylation (Figure 5m–p, quantification in U) (Paquet-Durand et al., 2007). Since the corresponding enzyme poly-ADP-ribose-polymerase (PARP) is activated upon DNA damage (De Vos et al., 2012), this observation indicates that photoreceptor DNA had become extensively damaged and is compatible with the DNA alkylating effect of STZ.

3.6 | Hemi-channels and endocytosis mediate STZ uptake into photoreceptors

The unexpected finding that STZ had essentially no effect on the viability of GLUT2 expressing HCs, while strongly increasing photoreceptor cell death, suggested that STZ taken up by HCs could be transported into photoreceptors. Feedback signalling from HCs to cone photoreceptors in the rodent retina has previously been shown (Liu et al., 2013; Szikra et al., 2014). Synaptic feedback mechanisms probably involve the transfer of small molecules between the synaptic cleft and the post-synaptic HC dendritic network via hemi-channels. These channels likely consist of connexins (Kamermans et al., 2001) and are sensitive to the connexin inhibitor meclofenamic acid (MFA) (Harks et al., 2001; Kemmler et al., 2014). Thus, to assess whether connexin-formed hemi-channels might be involved in the release of STZ from HC cytoplasm into the synaptic cleft, between HC and photoreceptors, we treated retinal explants with 100 μM MFA, in the presence or absence of 15 mM STZ.

Intriguingly, the negative effect of STZ on overall photoreceptor viability was mostly reverted by MFA treatment. When compared to control, application of 15 mM STZ to retinal explants strongly reduced photoreceptor survival, without affecting calbindin-stained HCs (Figure 6a, b). Treatment with 100 μM MFA alone did not seem to have an effect on photoreceptor or HC survival but blocked most of the detrimental effect of 15 mM STZ (Figure 6c, d). These results were corroborated by the results of the TUNEL staining for cell death (Figure 6g–j) and the corresponding quantifications of HCs, ONL thickness and percentage of TUNEL-positive cells (Figure 6s–u). Thus, the MFA treatment data support an uptake of STZ by GLUT2 into HCs and a subsequent
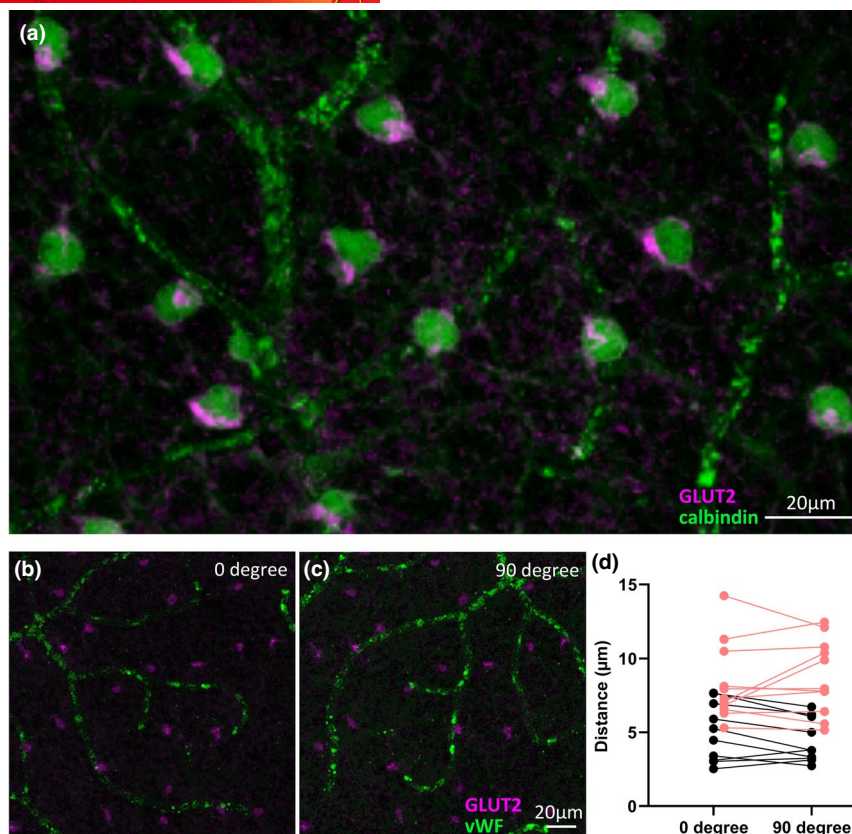
FIGURE 4 GLUT2 is expressed in close vicinity to inner retinal blood vessels. (a) Co-immunostaining for GLUT2 (magenta) and calbindin (green) on whole-mount retina, illustrating the proximity of horizontal cells (HCs) to the inner retinal vasculature. Note that the secondary anti-mouse IgG antibody used to detect calbindin also labelled the retinal vasculature. (b) Co-immunostaining for GLUT2 (magenta) and von Willebrand factor (vWF; green) on whole-mount retina showing the distribution of GLUT2 and blood vessels. (c) Image from B but with green channel rotated by 90 degrees. (d) Plot for the distances between HCs and blood vessels (black dots), and GLUT2-positive structures and vWF-positive vessels (red dots), in 0 degree and 90 degrees rotated images. Error bars: SD. For both comparisons Student´s paired t-test revealed no significant difference between groups. Images are representative for labelling performed on whole-mounted retina from five different animals

release of STZ from HCs into the synaptic cleft via connexin-formed hemi-channels.

To investigate how photoreceptors might take up the STZ extruded by HCs, we used dynasore (DYN), a dynamin GTPase inhibitor that blocks clathrin-mediated endocytosis (Macia et al., 2006). As for MFA, treatment with 50 μM DYN by itself did not significantly affect photoreceptor or HC viability, but when given together with 15 mM STZ it strongly reduced photoreceptor degeneration, as assessed by ONL thickness (Figure 6e, f) and the percentage of TUNEL-positive cells (Figure 6k, l). These results were suggestive of a hemi-channel-dependent export of STZ out of HCs and an uptake of STZ from the synaptic cleft into photoreceptor axon terminals via clathrin-mediated endocytosis.

However, this picture changed when we focused on cone photoreceptors in our analysis (Figure 6m–r, quantification in V): While 15 mM STZ abolished all cone photoreceptors as shown before (cf. Figure 5), MFA only partially reverted these negative effects. DYN, on the other hand, did not revert the negative effects of STZ on cone viability. What is more, DYN alone had clear detrimental effects on cone viability but not on overall photoreceptor viability, implying

that cones, but not rods, may depend more directly on clathrin-mediated endocytosis for their survival.

4 | DISCUSSION

Given the important role of glucose transport for retinal energy metabolism and disease pathogenesis, in this study, we sought to determine the cellular expression pattern and function of GLUT2 in the retina. We found GLUT2 to be strongly expressed in HCs, while, unexpectedly, treatment with the toxic GLUT2 substrate STZ caused dose-dependent photoreceptor degeneration, an effect that was more pronounced in cones. Blocking either hemi-channel function with MFA or endocytosis of photoreceptors with DYN strongly reduced the impact of STZ on rod photoreceptors, suggesting the existence of a transport mechanism for glucose, from HCs to photoreceptors. On the other hand, cone photoreceptor viability was negatively affected by DYN application, indicating that cones may rely much more than rods on synaptic glucose import for their survival. The detection of GLUT2 expression and the description of

FIGURE 5 Streptozotocin selectively ablates photoreceptors in a dose-dependent manner. Wild-type organotypic retinal explant cultures were treated with the GLUT2 selective drug streptozotocin (STZ) at concentrations of 1.5, 8 and 15 mM. (a–d) Calbindin-labelled horizontal cells (HC, green) were not significantly affected by STZ treatment (quantification in Q). (e–h) ONL thickness decreased in a concentration-dependent manner (quantified in R), while cell death (TUNEL assay, cyan) in the outer nuclear layer (ONL) increased (S). (i–l) At the same time, the number of cone photoreceptors, as assessed by cone arrestin labelling (magenta), strongly decreased with rising STZ levels (T). (m–p) Conversely, the accumulation of poly-ADP-ribose (black), as a surrogate marker for DNA damage, increased with the treatment (U). Error bars: SD. Statistical comparisons: (q–u): control vs. STZ treated using one-way ANOVA with Dunnett´s multiple-comparisons test. INL, inner nuclear layer. Images are representative for labelling performed on retinae from at least four different animals per treatment, DAPI (grey) was employed as nuclear counterstain
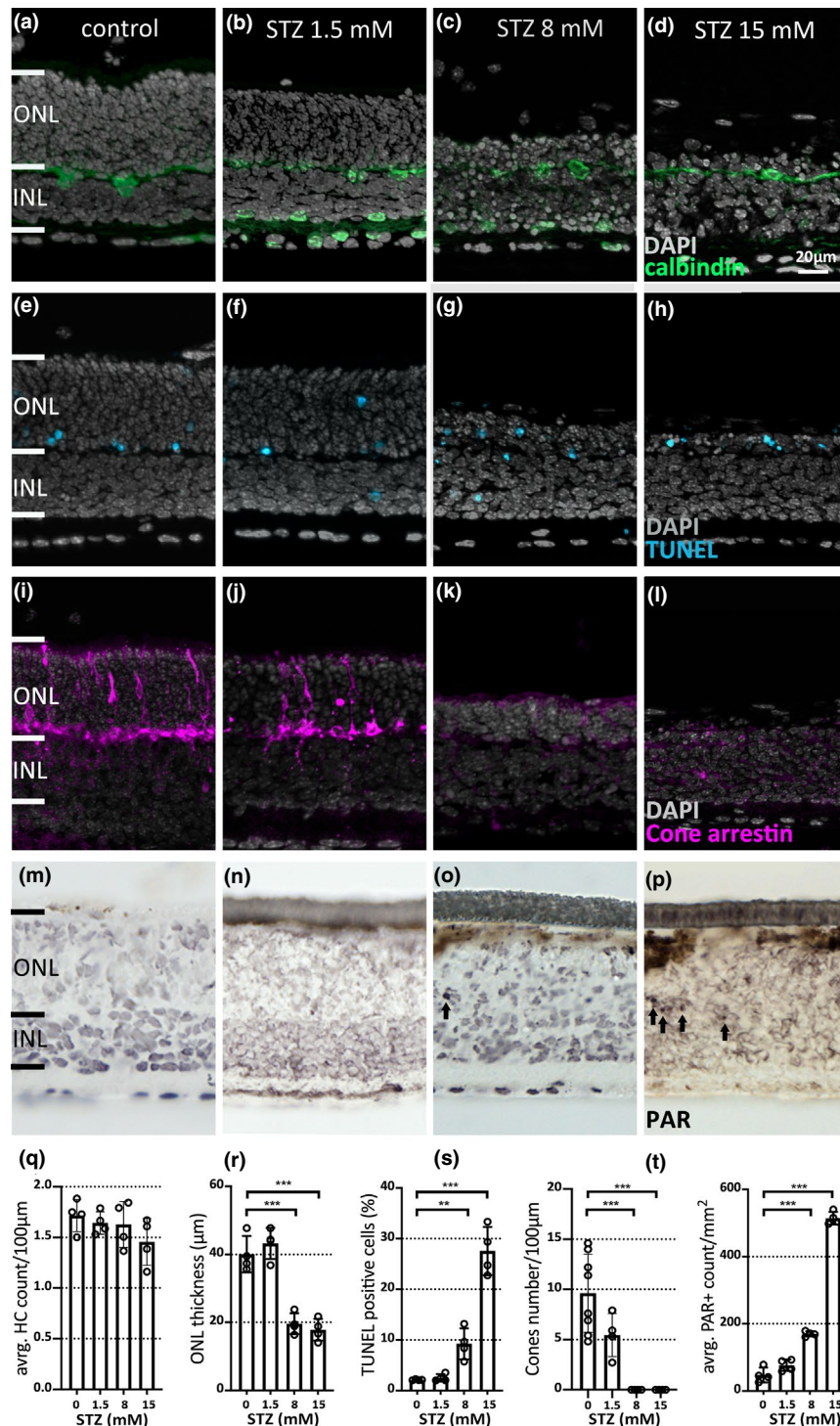
its function in the retina may be significant for the understanding of retinal energy metabolism and may have implications for animal studies which use STZ treatment as a means to induce diabetes.

4.1 | GLUT2 is expressed in horizontal cells of the mouse retina

The glucose transporter subtype GLUT2 is known to be expressed in liver, intestine, kidney and in pancreatic islet β-cells, as well as in the central nervous system, in neurons and in astrocytes (Bell et al., 1990; Koepsell, 2020). GLUT2 fulfils important roles in the regulation of metabolism, for instance intestinal GLUT2 regulates the absorption of glucose and contributes to the control of the tissue distribution of sugar absorbed from the diet (Boland et al., 2017; Schmitt et al., 2016). In the nervous system, GLUT2-dependent glucose sensing controls feeding, thermoregulation, as well as sympathetic and parasympathetic activity. Correspondingly, small populations of brain neurons are known to express GLUT2 (Tarussio et al., 2014; Thorens, 2014). In our study, we found GLUT2 to be strongly
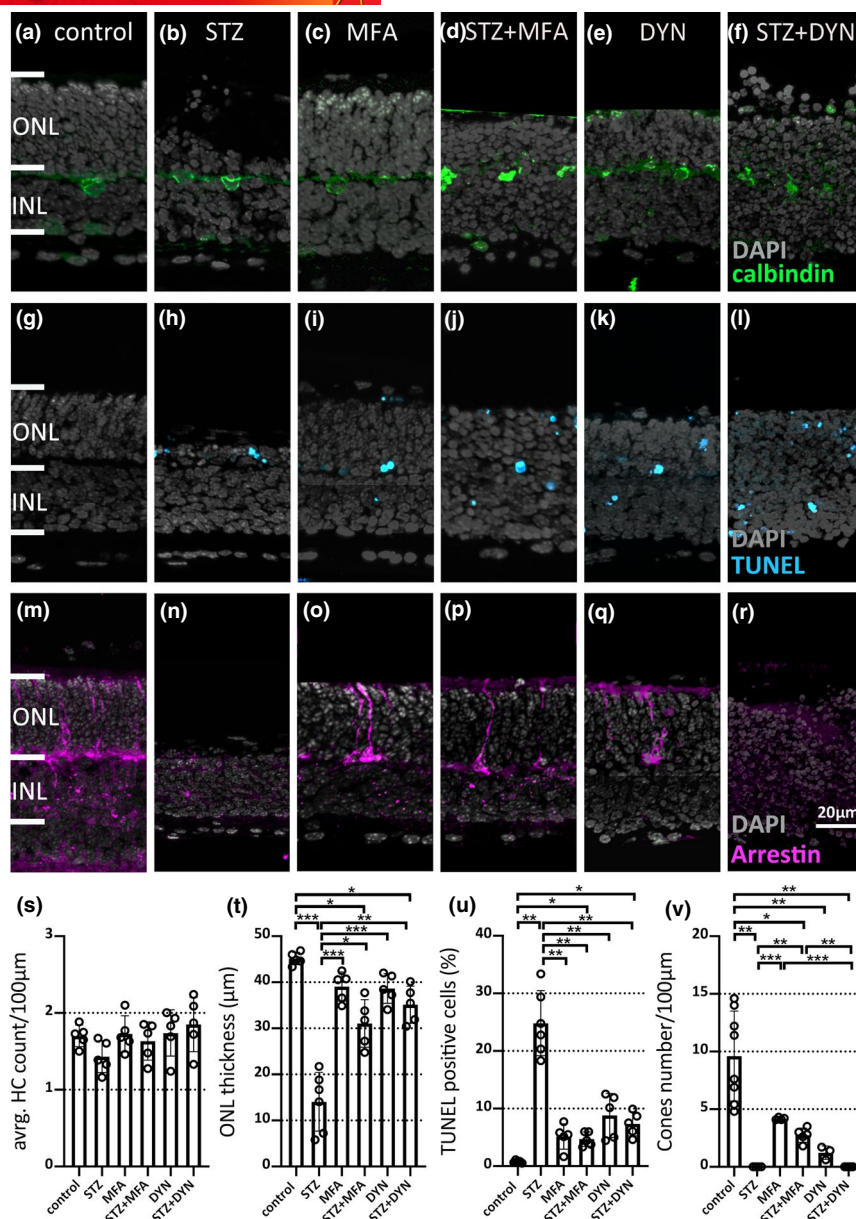
FIGURE 6 Inhibition of hemi-channels and endocytosis reduces streptozotocin toxicity. Wild-type organotypic retinal explant cultures were treated with either 15 mM streptozotocin (STZ), 100 μM meclofenamic acid (MFA), 50 μM dynasore (DYN), or combinations of these drugs. (a–f) When compared with control, ONL size was strongly decreased by 15 mM STZ, but not by 100 μM MFA. Combined MFA and STZ treatment had no effect on ONL thickness. Also 50 μM DYN did not negatively affect ONL size and neither did combined DYN and STZ treatment. Calbindin-labelled horizontal cells (HC, green) were not significantly affected by any of these treatments (HC quantification in S; ONL quantification in T). (g–l) The TUNEL assay (cyan) for cell death revealed a large proportion of dying cells in the ONL of STZ-treated retina, but fewer in MFA, MFA + STZ, DYN and DYN + STZ-treated explants (quantified in U). (m–r) Staining for the cone marker arrestin (magenta) showed that STZ application strongly decreased cone numbers, an effect that could not be rescued by application of either MFA or DYN (quantified in V). Error bars: SD. Statistical comparisons: (s–v): control vs. drug treated using a Brown-Forsythe and Welch ANOVA with Dunnett´s T3 multiple-comparisons test. INL, inner nuclear layer. Images are representative for labelling performed on retinae from five to six different animals per treatment, DAPI (grey) was employed as nuclear counterstain

and almost exclusively expressed in HCs of the mouse retina. Mouse HCs span the entire extent of the outer plexiform layer and their axonal and dendritic processes make synaptic connections with rod and cone photoreceptors respectively (Trumpler et al., 2008).

Our data showing that GLUT2-positive HCs are in close proximity to the inner retinal vasculature, is in agreement with

previous studies on mouse and rat retina, which showed that HCs form neurovascular units with the network of capillaries running through the OPL (Mojumder, 2008; Usui et al., 2015). Therefore, the connection between endothelial cell and HC on one side, and HC and photoreceptor on the other side, could potentially provide for efficient glucose transport from the blood stream into the

FIGURE 7 Proposed model for glucose transport from horizontal cell to photoreceptor synapse. In darkness, photoreceptor ribbon synapses require large amounts of energy to maintain their continuous glutamate release. In horizontal cells, GLUT2 allows glucose uptake, which may be re-released via hemi-channels located in the synaptic cleft. From there, photoreceptors (R, rod; C, cone) may use clathrin-mediated endocytosis to internalize glucose
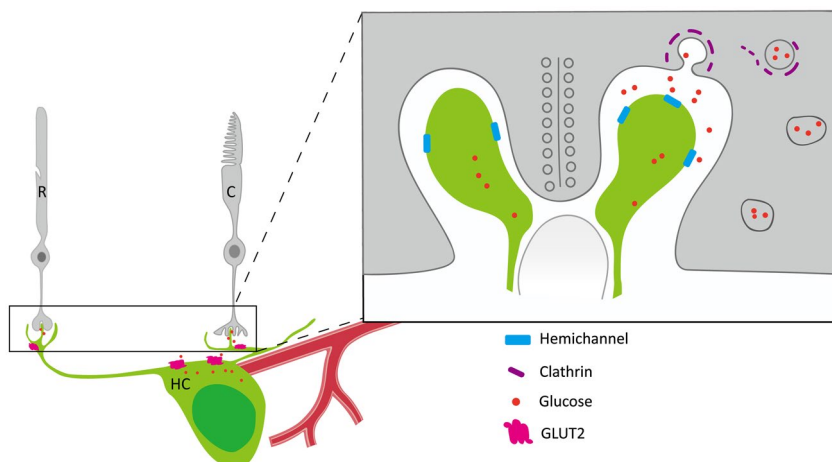
photoreceptor synapse. Intriguingly, in studies where HCs were genetically ablated, the architecture of the overall OPL was initially maintained, however, rod photoreceptors retracted their axons and degenerated partially, while cone photoreceptors appeared to be unaffected (Keeley et al., 2013; Sonntag et al., 2012). Moreover, when the connection between inner retinal vasculature and HCs was genetically disabled, rod photoreceptor degeneration in the *Pde6b*-mutant *rd10* mouse was accelerated (Usui et al., 2015). Hence, even under normal, physiological concentrations of glucose, HCs may play an important role for rod photoreceptor viability.

4.2 | STZ is toxic to photoreceptors: Evidence for retrograde glucose transport

STZ is an antibiotic that destroys pancreatic islet β-cells (Szkudelski, 2001). Due to its wide availability, cost-effectiveness, and relatively easy experimental handling, it is commonly used to generate animals that suffer from hyperglycaemia in a way that is similar to type-1 diabetes (Furman, 2015). Incidentally, the STZ model of diabetes has also been used extensively to study diabetic retinopathy (DR) (Aung et al., 2013; Liu et al., 2019; Zhang et al., 2019). The toxic effect of STZ on photoreceptors observed in this study warrants a note of caution when interpreting the results of such experiments. The maximal STZ dose used in our in vitro study on retinal explants was 15 mM, which is relatively high when compared to the doses that are usually used to render live animals diabetic (40–60 mg/kg, i.e. ≈0.2 mM). However, the STZ solutions administered *in vivo* via intravenous or intraperitoneal injection are far more concentrated, with typical concentrations ranging from 15 to 75 mM (4–20 mg/ml) (Furman, 2015). The highly perfused retina will likely be exposed to a disproportionately large amount of the drug. Thus, it is conceivable that STZ—when transported by GLUT2—may directly affect the retina, rather than indirectly via the hyperglycaemia caused by pancreatic beta cell destruction.

The effects of the STZ treatment are especially surprising since HCs, which express the STZ target GLUT2, are seemingly not affected, while photoreceptors—which do not appear to express GLUT2 at all—are severely affected. To explain this observation, we hypothesized that a transport mechanism exists, which allowed for STZ to move from HCs to photoreceptors. We first probed for such a mechanism using the blocker of connexin-formed hemi-channels MFA, which reverted the toxic effect of STZ on rod photoreceptors. This result indicates that the STZ taken up by HCs via GLUT2 could be exported via hemi-channels from the HC to the photoreceptor via the synaptic cleft (Kamermans et al., 2001). In a second instance, we blocked clathrin-mediated endocytosis using dynasore (Macia et al., 2006), which avoided STZ toxicity on rods, but which by itself had a deleterious effect on cones. Together, these data argue for a mechanism that makes use of hemi-channels and synaptic endocytosis to transport STZ from HCs to photoreceptors (Figure 7). It appears likely that such a mechanism will also apply to glucose transport. Indeed, the photoreceptor ribbon synapse differs from other synapses in the central nervous system in that, in darkness, it constantly releases the neurotransmitter glutamate. This constant release creates a large energy demand, both to produce ATP and glutamate (Ingram et al., 2020), that may be difficult to satisfy if relying only on glucose import from the outer retinal vasculature. Yet, no dedicated glucose transporter is known to be expressed in the photoreceptor synapse. Since glucose is non-electrogenic and non-protonogenic its release into the synaptic cleft and subsequent import into the photoreceptor synapse would not interfere with ephaptic feedback (Vroman et al., 2014). It is thus conceivable that glucose piggybacks on the ephaptic feedback pathway, to allow energy supply to the synapse without requiring a dedicated glucose transporter.

4.3 | Importance for diabetic retinopathy and retinal degeneration

Because energy metabolism is critical for cell survival, its alterations frequently cause disease, among which diabetes is a prominent example. Diabetes is a chronic disease characterized by defective insulin-signalling and exceedingly high and variable levels of glucose in the blood stream. DR is a complication of diabetes that affects

the retina in a high percentage of diabetics (Antonetti et al., 2012). The disease is associated with a variety of pathophysiological events such as microaneurysms, neovascularization and photoreceptor degeneration, which eventually lead to irreversible blindness (Cai & Boulton, 2002). In DR, colour vision is regularly affected early on, even when obvious signs of DR are not (yet) present (Roy et al., 1986; Wolff et al., 2015). Hence, cones appear to be particularly vulnerable to changes in glucose metabolism. Our data on the more marked vulnerability of cones to STZ treatment suggest an increased internalization of glucose in the large cone synapses. This is in line with work on salamander cones where the rate of synaptic vesicle internalization was found to be faster than in rods, thus allowing for increased uptake via this pathway (Van Hook & Thoreson, 2012).

On the other hand, rod photoreceptors degenerate in part in the absence of HC, while cone photoreceptors appear to be less dependent on HC function (Keeley et al., 2013; Sonntag et al., 2012). Under diabetic conditions, with elevated levels of glucose in the bloodstream, transport of glucose from HCs into photoreceptors may over-load cellular metabolism, causing a surge in reactive oxygen species and eventually photoreceptor degeneration. Indeed, high levels of glucose were found to be toxic to photoreceptors, and especially so to cones (Calbiague et al., 2020; Valdes et al., 2016), and it is plausible that a part of this detrimental effect may stem from GLUT2 activity in HC. This in turn suggests that modulation of GLUT2 transport may be considered for therapeutic purposes.

5 | CONCLUSION

Knowledge on the expression and functioning of glucose transporters in the retina is crucial to further our understanding of retinal energy metabolism. Here, we showed that GLUT2 is prominently expressed in HCs of the mouse retina, and we propose a role for this transporter in a putative glucose shuttle, from HCs to photoreceptors. The discovery of this new pathway is likely to be relevant for future studies into retinal disease pathogenesis, including for DR. Moreover, while the compound STZ is widely used to destroy insulin-producing β-cells and generate diabetic animals, the direct adverse effects of STZ on photoreceptors highlight the need for careful evaluation of research results obtained in STZ-treated animals.

CONFLICT OF INTEREST

The authors declare no conflicts of interest.

AUTHORS' CONTRIBUTIONS

FPD, KJ and ZH designed research; MY, YC, SV and EK performed research; MY, YC, SV and EK analysed data; MY, YC, FPD, OS, MU and KJ wrote the paper.

DATA AVAILABILITY STATEMENT

Data are available in the article's supplementary material.

ORCID

Yiyi Chen https://orcid.org/0000-0002-9007-4227
Stavros Vagionitis https://orcid.org/0000-0002-9501-0695
Kangwei Jiao https://orcid.org/0000-0003-3202-5993
François Paquet-Durand https://orcid.org/0000-0001-7355-5742

REFERENCES

Aït-Ali, N., Fridlich, R., Millet-Puel, G., Clérin, E., Delalande, F., Jaillard, C., Blond, F., Perrocheau, L., Reichman, S., Byrne, L. C., Olivier-Bandini, A., Bellalou, J., Moyse, E., Bouillaud, F., Nicol, X., Dalkara, D., van Dorsselaer, A., Sahel, J.-A., & Léveillard, T. (2015). Rod-derived cone viability factor promotes cone survival by stimulating aerobic glycolysis. *Cell*, 161, 817–832. https://doi.org/10.1016/j.cell.2015.03.023

Antonetti, D. A., Klein, R., & Gardner, T. W. (2012). Diabetic retinopathy. *New England Journal of Medicine*, 366, 1227–1239. https://doi.org/10.1056/NEJMra1005073

Aung, M. H., Kim, M. K., Olson, D. E., Thule, P. M., & Pardue, M. T. (2013). Early visual deficits in streptozotocin-induced diabetic long evans rats. *Investigative Ophthalmology & Visual Science*, 54, 1370–1377. https://doi.org/10.1167/iovs.12-10927

Belhadj, S., Tolone, A., Christensen, G., Das, S., Chen, Y., & Paquet-Durand, F. (2020). Long-term, serum-free cultivation of organotypic mouse retina explants with intact retinal pigment epithelium. *Journal of Visualized Experiments: Jove*. https://doi.org/10.3791/61868

Bell, G. I., Kayano, T., Buse, J. B., Burant, C. F., Takeda, J., Lin, D., Fukumoto, H., & Seino, S. (1990). Molecular biology of mammalian glucose transporters. *Diabetes Care*, 13, 198–208. https://doi.org/10.2337/diacare.13.3.198

Boland, B. B., Rhodes, C. J., & Grimsby, J. S. (2017). The dynamic plasticity of insulin production in β-cells. *Molecular Metabolism*, 6, 958–973. https://doi.org/10.1016/j.molmet.2017.04.010

Bowes, C., Li, T., Danciger, M., Baxter, L. C., Applebury, M. L., & Farber, D. B. (1990). Retinal degeneration in the rd mouse is caused by a defect in the beta subunit of rod cGMP-phosphodiesterase. *Nature*, 347, 677–680.

Brosky, G., & Logothetopoulos, J. (1969). Streptozotocin diabetes in the mouse and guinea pig. *Diabetes*, 18, 606–611. https://doi.org/10.2337/diab.18.9.606

Caffe, A. R., Ahuja, P., Holmqvist, B., Azadi, S., Forsell, J., Holmqvist, I., Soderpalm, A. K., & van Veen, T. (2001). Mouse retina explants after long-term culture in serum free medium. *Journal of Chemical*

Neuroanatomy, 22, 263–273. https://doi.org/10.1016/S0891-0618(01)00140-5

Cai, J., & Boulton, M. (2002). The pathogenesis of diabetic retinopathy: Old concepts and new questions. *Eye (Lond)*, 16, 242–260. https://doi.org/10.1038/sj.eye.6700133

Calbiague, V. M., Vielma, A. H., Cadiz, B., Paquet-Durand, F., & Schmachtenberg, O. (2020). Physiological assessment of high glucose neurotoxicity in mouse and rat retinal explants. *The Journal of Comparative Neurology*, 528, 989–1002. https://doi.org/10.1002/cne.24805

Chen, Z., Wang, J., Sun, W., Archibong, E., Kahkoska, A. R., Zhang, X., Lu, Y., Ligler, F. S., Buse, J. B., & Gu, Z. (2018). Synthetic beta cells for fusion-mediated dynamic insulin secretion. *Nature Chemical Biology*, 14, 86–93. https://doi.org/10.1038/nchembio.2511

De Vos, M., Schreiber, V., & Dantzer, F. (2012). The diverse roles and clinical relevance of PARPs in DNA damage repair: current state of the art. *Biochemical Pharmacology*, 84, 137–146.

Furman, B. L. (2015). Streptozotocin-induced diabetic models in mice and rats. *Current Protocols in Pharmacology*, 70, 41–45. https://doi.org/10.1002/0471141755.ph0547s70

Halperin, D. M., Kulke, M. H., & Yao, J. C. (2015). A tale of two tumors: Treating pancreatic and extrapancreatic neuroendocrine tumors. *Annual Review of Medicine*, 66, 1–16. https://doi.org/10.1146/annurev-med-061813-012908

Harks, E. G., de Roos, A. D., Peters, P. H., de Haan, L. H., Brouwer, A., Ypey, D. L., van Zoelen, E. J., & Theuvenet, A. P. (2001). Fenamates: A novel class of reversible gap junction blockers. *Journal of Pharmacology and Experimental Therapeutics*, 298, 1033–1041.

Haverkamp, S., & Wassle, H. (2000). Immunocytochemical analysis of the mouse retina. *The Journal of Comparative Neurology*, 424, 1–23. https://doi.org/10.1002/1096-9861(20000814)424:1<1:AID-CNE1>3.0.CO;2-V

Ingram, N. T., Fain, G. L., & Sampath, A. P. (2020). Elevated energy requirement of cone photoreceptors. *Proceedings of the National Academy of Sciences*, 117, 19599–19603. https://doi.org/10.1073/pnas.2001776117

Kamermans, M., Fahrenfort, I., Schultz, K., Janssen-Bienhold, U., Sjoerdsma, T., & Weiler, R. (2001). Hemichannel-mediated inhibition in the outer retina. *Science*, 292, 1178–1180. https://doi.org/10.1126/science.1060101

Kanow, M. A., Giarmarco, M. M., Jankowski, C. S. R., Tsantilas, K., Engel, A. L., Du, J., Linton, J. D., Farnsworth, C. C., Sloat, S. R., Rountree, A., Sweet, I. R., Lindsay, K. J., Parker, E. D., Brockerhoff, S. E., Sadilek, M., Chao, J. R., & Hurley, J. B. (2017). Biochemical adaptations of the retina and retinal pigment epithelium support a metabolic ecosystem in the vertebrate eye. *Elife*, 6, e28899. https://doi.org/10.7554/eLife.28899

Keeler, C. E. (1924). The inheritance of a retinal abnormality in white mice. *Proceedings of the National Academy of Sciences of the United States of America*, 10, 329–333.

Keeley, P. W., Luna, G., Fariss, R. N., Skyles, K. A., Madsen, N. R., Raven, M. A., Poche, R. A., Swindell, E. C., Jamrich, M., Oh, E. C., Swaroop, A., Fisher, S. K., & Reese, B. E. (2013). Development and plasticity of outer retinal circuitry following genetic removal of horizontal cells. *The Journal of Neuroscience: the Official Journal of the Society for Neuroscience*, 33, 17847–17862. https://doi.org/10.1523/JNEUROSCI.1373-13.2013

Kemmler, R., Schultz, K., Dedek, K., Euler, T., & Schubert, T. (2014). Differential regulation of cone calcium signals by different horizontal cell feedback mechanisms in the mouse retina. *Journal of Neuroscience*, 34, 11826–11843. https://doi.org/10.1523/JNEUROSCI.0272-14.2014

Koepsell, H. (2020). Glucose transporters in brain in health and disease. *Pflugers Archiv. European Journal of Physiology*, 472, 1299–1343. https://doi.org/10.1007/s00424-020-02441-x

Koukourakis, M. I., Giatromanolaki, A., Zois, C. E., Kalamida, D., Pouliliou, S., Karagounis, I. V., Yeh, T.-L., Abboud, M. I., Claridge, T. D. W., Schofield, C. J., Sivridis, E., Simopoulos, C., Tokmakidis, S. P., & Harris, A. L. (2016). Normal tissue radioprotection by amifostine via Warburg-type effects. *Scientific Reports*, 6, 30986. https://doi.org/10.1038/srep30986

Kovács-Öller, T., Szarka, G., Ganczer, A., Tengölics, Á., Balogh, B., & Völgyi, B. (2019). Expression of Ca2+-binding buffer proteins in the human and mouse retinal neurons. *International Journal of Molecular Sciences*, 20, 2229. https://doi.org/10.3390/ijms20092229

Liu, L., Jiang, Y., & Steinle, J. J. (2019). Epac1 and glycyrrhizin both inhibit HMGB1 levels to reduce diabetes-induced neuronal and vascular damage in the mouse retina. *Journal of Clinical Medicine*, 8(6), 772. https://doi.org/10.3390/jcm8060772

Liu, X., Hirano, A. A., Sun, X., Brecha, N. C., & Barnes, S. (2013). Calcium channels in rat horizontal cells regulate feedback inhibition of photoreceptors through an unconventional GABA- and pH-sensitive mechanism. *The Journal of Physiology*, 591, 3309–3324. https://doi.org/10.1113/jphysiol.2012.248179

Lund-Andersen, H. (1979). Transport of glucose from blood to brain. *Physiological Reviews*, 59(2), 305–352. https://doi.org/10.1152/physrev.1979.59.2.305

Macia, E., Ehrlich, M., Massol, R., Boucrot, E., Brunner, C., & Kirchhausen, T. (2006). Dynasore, a cell-permeable inhibitor of dynamin. *Developmental Cell*, 10, 839–850. https://doi.org/10.1016/j.devcel.2006.04.002

Mantych, G. J., Hageman, G. S., & Devaskar, S. U. (1993). Characterization of glucose transporter isoforms in the adult and developing human eye. *Endocrinology*, 133, 600–607. https://doi.org/10.1210/endo.133.2.8344201

Mojumder, D. K. (2008). Capillary-contacting horizontal cells in the rodent retina. *Journal of the Anatomical Society India*, 57, 34–36.

Paquet-Durand, F., Silva, J., Talukdar, T., Johnson, L. E., Azadi, S., van Veen, T., Ueffing, M., Hauck, S. M., & Ekstrom, P. A. (2007). Excessive activation of poly(ADP-ribose) polymerase contributes to inherited photoreceptor degeneration in the retinal degeneration 1 mouse. *Journal of Neuroscience*, 27, 10311–10319. https://doi.org/10.1523/JNEUROSCI.1514-07.2007

Peichl, L. (2005). Diversity of mammalian photoreceptor properties: Adaptations to habitat and lifestyle? *The Anatomical Record Part A: Discoveries in Molecular, Cellular, and Evolutionary Biology*, 287A, 1001–1012. https://doi.org/10.1002/ar.a.20262

Power, M., Das, S., Schutze, K., Marigo, V., Ekstrom, P., & Paquet-Durand, F. (2020). Cellular mechanisms of hereditary photoreceptor degeneration—Focus on cGMP. *Progress in Retinal and Eye Research*, 74, 100772. https://doi.org/10.1016/j.preteyeres.2019.07.005

Roy, M. S., Gunkel, R. D., & Podgor, M. J. (1986). Color vision defects in early diabetic retinopathy. *Archives of Ophthalmology*, 104, 225–228. https://doi.org/10.1001/archopht.1986.01050140079024

Sanyal, S., & Bal, A. K. (1973). Comparative light and electron microscopic study of retinal histogenesis in normal and rd mutant mice. *Zeitschrift Anatomie und Entwicklungsgeschichte*, 142, 219–238. https://doi.org/10.1007/BF00519723

Schmitt, C. C., Aranias, T., Viel, T., Chateau, D., Le Gall, M., Waligora-Dupriet, A.-J., Melchior, C., Rouxel, O., Kapel, N., Gourcerol, G., Tavitian, B., Lehuen, A., Brot-Laroche, E., Leturque, A., Serradas, P., & Grosfeld, A. (2016). Intestinal invalidation of the glucose transporter GLUT2 delays tissue distribution of glucose and reveals an unexpected role in gut homeostasis. *Molecular Metabolism*, 6, 61–72. https://doi.org/10.1016/j.molmet.2016.10.008

Schnedl, W. J., Ferber, S., Johnson, J. H., & Newgard, C. B. (1994). STZ transport and cytotoxicity. Specific enhancement in GLUT2-expressing cells. *Diabetes*, 43, 1326–1333. https://doi.org/10.2337/diab.43.11.1326

Sonntag, S., Dedek, K., Dorgau, B., Schultz, K., Schmidt, K.-F., Cimiotti, K., Weiler, R., Lowel, S., Willecke, K., & Janssen-Bienhold, U.

(2012). Ablation of retinal horizontal cells from adult mice leads to rod degeneration and remodeling in the outer retina. *Journal of Neuroscience*, 32, 10713–10724. https://doi.org/10.1523/JNEUROSCI.0442-12.2012

Szikra, T., Trenholm, S., Drinnenberg, A., Jüttner, J., Raics, Z., Farrow, K., Biel, M., Awatramani, G., Clark, D. A., Sahel, J.-A., da Silveira, R. A., & Roska, B. (2014). Rods in daylight act as relay cells for cone-driven horizontal cell-mediated surround inhibition. *Nature Neuroscience*, 17, 1728–1735. https://doi.org/10.1038/nn.3852

Szkudelski, T. (2001). The mechanism of alloxan and streptozotocin action in B cells of the rat pancreas. *Physiological Research*, 50, 537–546.

Tarussio, D., Metref, S., Seyer, P., Mounien, L., Vallois, D., Magnan, C., Foretz, M., & Thorens, B. (2014). Nervous glucose sensing regulates postnatal beta cell proliferation and glucose homeostasis. *Journal of Clinical Investigation*, 124, 413–424.

Thorens, B. (2014). Neural regulation of pancreatic islet cell mass and function. *Diabetes, Obesity & Metabolism*, 16(Suppl 1), 87–95. https://doi.org/10.1111/dom.12346

Thorens, B. (2015). GLUT2, glucose sensing and glucose homeostasis. *Diabetologia*, 58, 221–232. https://doi.org/10.1007/s00125-014-3451-1

Trick, G. L., & Berkowitz, B. A. (2005). Retinal oxygenation response and retinopathy. *Progress in Retinal and Eye Research*, 24, 259–274. https://doi.org/10.1016/j.preteyeres.2004.08.001

Trumpler, J., Dedek, K., Schubert, T., de Sevilla Muller, L. P., Seeliger, M., Humphries, P., Biel, M., & Weiler, R. (2008). Rod and cone contributions to horizontal cell light responses in the mouse retina. *Journal of Neuroscience*, 28, 6818–6825. https://doi.org/10.1523/JNEUROSCI.1564-08.2008

Usui, Y., Westenskow, P. D., Kurihara, T., Aguilar, E., Sakimoto, S., Paris, L. P., Wittgrove, C., Feitelberg, D., Friedlander, M. S. H., Moreno, S. K., Dorrell, M. I., & Friedlander, M. (2015). Neurovascular crosstalk between interneurons and capillaries is required for vision. *Journal of Clinical Investigation*, 125, 2335–2346. https://doi.org/10.1172/JCI80297

Valdes, J., Trachsel-Moncho, L., Sahaboglu, A., Trifunovic, D., Miranda, M., Ueffing, M., Paquet-Durand, F., & Schmachtenberg, O. (2016). Organotypic retinal explant cultures as in vitro alternative for diabetic retinopathy studies. *Altex*, 33, 459–464. https://doi.org/10.14573/altex.1603111

Van Hook, M. J., & Thoreson, W. B. (2012). Rapid synaptic vesicle endocytosis in cone photoreceptors of salamander retina. *Journal of Neuroscience*, 32, 18112–18123. https://doi.org/10.1523/JNEUROSCI.1764-12.2012

Vighi, E., Trifunović, D., Veiga-Crespo, P., Rentsch, A., Hoffmann, D., Sahaboglu, A., Strasser, T., Kulkarni, M., Bertolotti, E., van den Heuvel, A., Peters, T., Reijerkerk, A., Euler, T., Ueffing, M., Schwede, F., Genieser, H.-G., Gaillard, P., Marigo, V., Ekström, P., & Paquet-Durand, F. (2018). Combination of cGMP analogue and drug delivery system provides functional protection in hereditary retinal degeneration. *Proceedings of the National Academy of Sciences*, 115, E2997–E3006. https://doi.org/10.1073/pnas.1718792115

Vroman, R., Klaassen, L. J., Howlett, M. H., Cenedese, V., Klooster, J., Sjoersdma, T., & Kamermans, M. (2014). Extracellular ATP hydrolysis inhibits synaptic transmission by increasing ph buffering in the synaptic cleft. *PLoS Biology*, 12, e1001864. https://doi.org/10.1371/journal.pbio.1001864

Watanabe, T., Mio, Y., Hoshino, F. B., Nagamatsu, S., Hirosawa, K., & Nakahara, K. (1994). GLUT2 expression in the rat retina: Localization at the apical ends of Müller cells. *Brain Research*, 655, 128–134. https://doi.org/10.1016/0006-8993(94)91606-3

Watanabe, T., Nagamatsu, S., Matsushima, S., Kondo, K., Motobu, H., Hirosawa, K., Mabuchi, K., Kirino, T., & Uchimura, H. (1999). Developmental expression of GLUT2 in the rat retina. *Cell and Tissue Research*, 298, 217–223. https://doi.org/10.1007/s004419900099

Wolff, B. E., Bearse, M. A. Jr, Schneck, M. E., Dhamdhere, K., Harrison, W. W., Barez, S., & Adams, A. J. (2015). Color vision and neuroretinal function in diabetes. *Documenta Ophthalmologica. Advances in Ophthalmology*, 130, 131–139.

Zhang, T., Ouyang, H., Mei, X., Lu, B., Yu, Z., Chen, K., Wang, Z., & Ji, L. (2019). Erianin alleviates diabetic retinopathy by reducing retinal inflammation initiated by microglial cells via inhibiting hyperglycemia-mediated ERK1/2-NF-kappaB signaling pathway. *The FASEB Journal*, 33, 11776–11790.

SUPPORTING INFORMATION

Additional supporting information may be found in the online version of the article at the publisher's website.